

Memory in cyclically crumpled sheets

Amit Dawadi and Arshad Kudrolli

Department of Physics, Clark University, Worcester, Massachusetts 01610, USA

(Dated: April 2, 2024)

We investigate the crumpling of a sheet as it is repeatedly crushed onto itself by rolling it into a cylinder and twisting it axially while allowing the end-to-end length to evolve freely. As deduced from its plastic deformations, the sheet creases and collapses into structures which repeat and sharpen over hundreds of cycles to a remarkable degree before forming new configurations. The observed metastability increases with applied cycles leading to recurrent structures over a significant range of loading before the sheet tears, but reconfigurations continue to occur for large enough loading amplitude. The evolution of the sheet structure as measured by the mean curvature and the total crease length is found to increase logarithmically with cycle number with a rate which increases with degree of compression. We explain the overall extent of creasing using flat folding models, and show the logarithmic growth as being a consequence of individual creases becoming sharper with number of folding cycles, and due to the bifurcation in the curvature field leading to the formation of new creases and folding pathways. Thus, we show that elastoplastic sheets can follow complex folding pathways to form convergent structures after a sufficiently large number of training cycles provided material fatigue remains unimportant.

I. INTRODUCTION

A crumpled sheet shows a distinct pattern of intersecting creases which carry the subtle imprints of the complex buckling pathways followed as a result of applied constraints [1–5]. The evolution of the observed disordered ridges and facets can provide broad lessons on a system that can typically only access metastable states [6–8]. While there have been considerable number of experimental and theoretical studies on memory effects after the application or removal of stress [9–12], the evolution under repeated loading cycles has only started garnering attention more recently. As a result of sensitive dependence on the loading conditions, the sheet cannot be expected to pass the same path if the sheet is crumpled again, thus leading to further creases and hysteresis [13, 14]. Nonetheless, the presence of creases influences how the sheet subsequently collapses when the loading cycle is repeated as the sheet rigidifies along the length of the crease, while becoming easier to fold about the crease [15], leading to guided folding pathways as in origami [16]. Indeed, supervised strengthening folds and weakening of misfolds in a repeatedly crumpled sheet has been suggested as a paradigm for reinforced learning of structures in mechanical systems subjected to classes of forces [17]. It has been argued based on numerical simulations, that the energy landscape of a folded sheet can become deeper under repeated loading, driving the sheet to unique folding pathways even under unsupervised conditions [18]. However, investigations of these ideas have been conducted with actual sheets remain limited [19].

In the case of athermal granular systems, logarithmic relaxation of observables such as density can occur upon application of thousands of vibration cycles [20]. It has been also shown that reversible motion and relaxation to limit cycle can be observed in cyclically sheared colloidal suspensions and amorphous solids that show irreversible motion above a critical amount of deformation [21, 22]. In the case of a pre-crumpled sheet under repeated loading and unloading, hysteresis and an approach to a limit cycle have been observed when the loading is below the threshold required to create additional crumples [23]. But, even a pre-creased ordered origami can snap between different deployed structures because of their multistability [24–26]. Furthermore, even single folds in elastoplastic sheets can age [11, 24] impacting their compaction properties [27, 28]. Thus, the evolution of the crumpled structure of a sheet subject to large number of repeated loading and unloading cycles of varying strength, remains unclear.

To address the evolution of an elastoplastic sheet subject to large number of training cycles, we examine the crumpling of a Mylar sheet which is clamped onto circular end caps, and then repeatedly crushed by applying an axial twist akin to wringing a towel [29]. Because of the inextensible nature of the sheet, its length contracts axially, and the sheet collapses onto itself while forming a bundle [30]. A hallmark of our design is that the applied strain can be reversed back to zero, and thus the loading cycle can be repeated essentially indefinitely under well prescribed conditions. This system enables us to examine the effect of sheet training over a wide range of compaction before material fatigue leads to fractures or tears in the sheet. Because no constraint is imposed on the end-to-end distance, it can serve as a measure of the macroscopic state of the system, which can evolve with cycle number, enabling a subtle examination of the effect of cyclic loading. The broad question we seek to understand is whether convergent structures can be observed under unsupervised training cycles, and if so under what range of conditions. As we discuss in the following, the sheets fold to form increasingly long-lived metastable structures over sufficiently large number of loading cycles even as the system ages logarithmically.

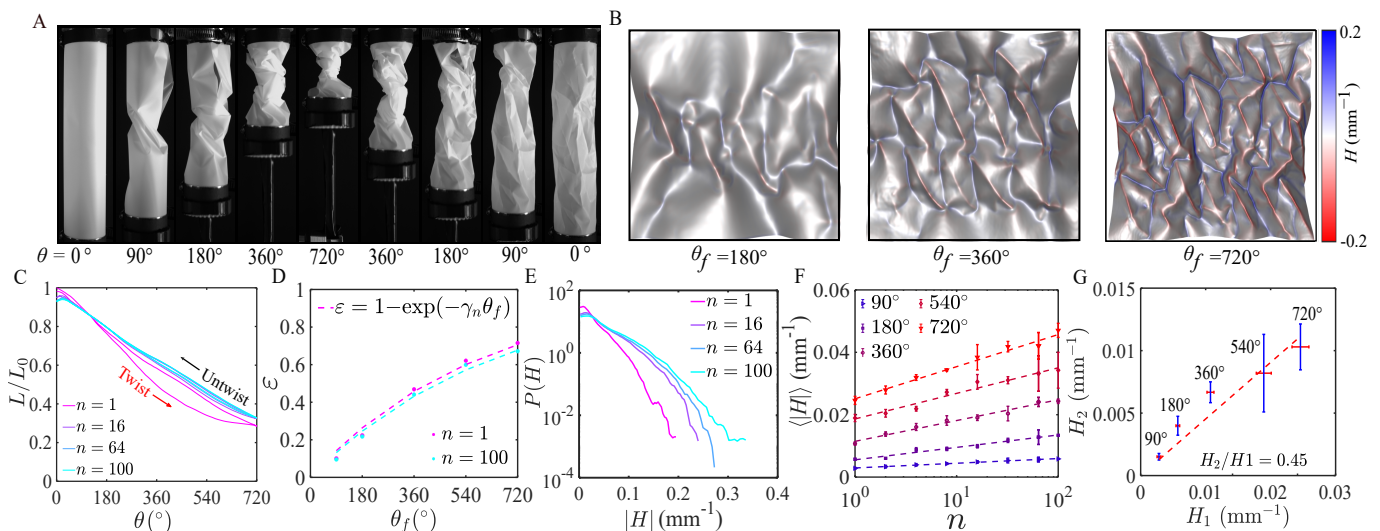


FIG. 1. Crumpling of an elastoplastic sheet with a twist. (A) Images of a sheet ($L_0 = 16.5$ cm, $W_0 = 16.5$ cm, and $h = 90$ μm) as it is twisted and then untwisted about its axis through $\theta_f = 720^\circ$. (B) The crumples observed after one cycle corresponding to various θ_f . The mean curvature H are superimposed with values denoted by the color bar. (C) The end-to-end length L as a function of θ shows hysteresis which decreases with n . (D) The strain ε versus θ_f can be described by the exponential function $\varepsilon = 1 - \exp(-\gamma_n \theta_f)$ with $1/\gamma_1 = 588^\circ$ and $1/\gamma_{100} = 636^\circ$ corresponding $n = 1$ and 100, respectively. (E) The distribution of the magnitude of the mean curvature $|H|$ broadens with n . (F) The evolution of the average magnitude of mean curvature $\langle |H| \rangle$ with n is described by a logarithmic function $\langle |H| \rangle = H_1 + H_2 \log n$. (G) H_1 and H_2 increase with increasing θ_f .

II. CRUMPLING BY TWISTING

Figure 1A shows the evolution of a sheet as it is twisted quasi-statically up to an axial angle $\theta_f = 720^\circ$, and then untwisted (see Methods). As the twist angle θ is increased, the sheet is observed to buckle with folds slanted along the direction of twist in the central section between the clamps ends, while the sections close to the clamps remain relatively cylindrical [31, 32]. Thus, the twisting is observed to lead to the self-collapse and contraction of the sheet which is not directly imposed by an inward moving bounding surface as in a piston [13]. The buckling instability is similar to those found in twisted long cylindrical shells [33] (see Supplementary Information (SI) Section I). As the twist is increased further, self-contact occurs, the initial folds split, and the sheet crumples. When the applied twist is reversed, the crumpled structure show auxetic behavior [34] with increases in both length and diameter as the sheet returns back close to its initial cylindrical shape as the elastic components of folds relax while showing imprints of plastic deformation. When the twist cycle is repeated, one notes that the sheets folds largely along creases which were formed during the first cycle (see Supplementary Movie S1).

Figure 1B shows scans of the sheet for increasing θ_f using laser profilometry (see Methods) rendered with color corresponding to local mean curvature of the surface H . In the case of $\theta_f = 180^\circ$, imprints of the initial folds that form can be observed even as the sheet comes into self-contact and the folds start to bend and break to accommodate the increasing twist. The sheet is observed to become more widely creased and disordered as θ_f is increased to 360° and $\theta_f = 720^\circ$. Thus, elastoplastic sheets become disordered, unlike hyperelastic sheets which show ordered folds corresponding to Schläfli symbols when twisted through similar θ [35]. We further find that the crumpled structure largely repeated itself after application of a full cycle with increasing n . But, formation of new creases and slow evolution of overall structure can be also observed (Supplementary Movie S2). In the following, we characterize and quantify the evolution of the system with n as a function of the degree of compaction by varying θ_f .

We quantify the strain experienced by the system using the end-to-end length L of the sheet from one clamp edge to the other, and plot it in Fig. 1C as a function of θ . L decreases faster with θ compared to a set of infinitesimally thin inextensible strings that initially form a hyperbolic hyperboloid (see SI Section II and SI Fig. S2). While untwisting, L increases but follows a different path which is systematically higher compared to the twisting phase, before crossing and reaching a length L_n which is slightly below L_0 . When the sheet is again subjected to the same cycle, the hysteresis is observed to decrease on average with each cycle (see Fig. 1C), while the length after a cycle continues to contract (see SI Section III). We characterize the compression of the sheet by measuring the end to end length L_c when θ_f is reached, and calculating the axial strain $\varepsilon = 1 - L_c/L_0$, and plotting it averaged over 3 trails versus θ in Fig. 1D. We observe that its increase can be described with the function $\varepsilon = 1 - \exp(-\gamma_n \theta_f)$, where γ_n decreases

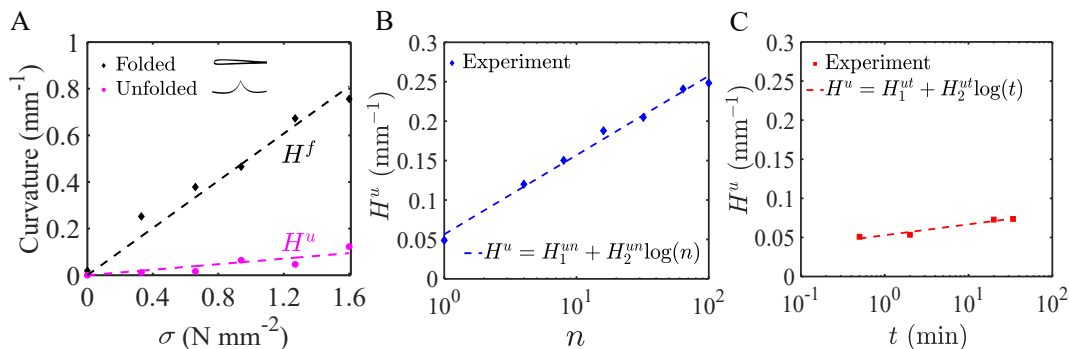


FIG. 2. Evolution of crease curvature with applied loading. (A) The mean curvature of a fold H^f in sheet which is folded in half as a function of applied force per unit cross section area, and the corresponding mean curvature after the sheet is unfolded H^u to measure the resulting plastic deformation ($L_0 = 16.5$ cm). A fit to $H^f = \chi^f \sigma$ and $H^u = \chi^u \sigma$ with $\chi^f = 0.5 \text{ mmN}^{-1}$ and $\chi^u = 0.06 \text{ mmN}^{-1}$, respectively, are shown. Inset: A cross section of the folded and unfolded sheets are also shown. (B) H^u as a function of n ($\sigma = 0.7 \text{ Nmm}^{-2}$; $T = 30$ seconds). A fit to $H^u = H_1^{un} + H_2^{un} \log(n)$ is shown with $H_1^{un} = 0.049 \text{ mm}^{-1}$ and $H_2^{un} = 0.10 \text{ mm}^{-1}$. (C) H^u increases as a function of time interval over which the same constant force is applied. A function $H^u = H_1^{ut} + H_2^{ut} \log(t)$ is shown with $H_1^{ut} = 0.051 \text{ mm}^{-1}$ at $t = 30$ seconds and $H_2^{ut} = 0.014 \text{ mm}^{-1} \text{ min}^{-1}$ is shown. The effect on H^u is significantly lower over t compared with n while considering the same time taken to apply the loading cycles.

slowly with n as the plastic deformation in the sheet accumulate. The exponential function is consistent with the sheet becoming increasingly more difficult to compress with increasing compaction.

To quantify the evolution with applied loading cycles, we obtain the distributions of the magnitude of the local mean curvature $P(|H|)$ and plot them in Fig. 1E for various n . We observe that it is broadly distributed, and broadens further as the sheet is repeatedly twisted showing that the sheet is being increasingly creased not only with θ_f (see SI Section III), but with n as well (see SI Movie S2). We plot the average of the distribution $\langle |H| \rangle$ in Fig. 1F and observe that $\langle |H| \rangle$ grows systematically higher with increasing θ_f . Further, each $\langle |H| \rangle$ is well described by a logarithmic function $\langle |H| \rangle = H_1 + H_2 \log n$, where H_1 is the magnitude of the mean curvature observed after the application of the first cycle, and H_2 captures the growth with number of cycles. As shown in Fig. 1G, H_2 increasing approximately proportional to H_1 . Thus, we find that not only do the crumples formed depend on the applied twist, but that the rate of the grow upon repeated loading is essentially proportional the creases formed initially.

III. LOGARITHMIC GROWTH OF CURVATURE

We examine the curvature of a single crease upon repeated folding as a starting point to understand the logarithmic growth, and any relation to Arrhenius behavior that has been observed in response to application of stress in crumpled sheets [11, 12, 36, 37]. While the slow relaxation of a fold after application of a stress and its functional form as a function of time has been well studied [11, 36], the functional evolution of the fold over a large number of training cycles is not available. Therefore, a folded sheet is placed between parallel plates and a normal force is applied for a fixed time, and the force is then removed to relax the elastic component of the crease and the unfolded sheet is placed on a flat-bed for scanning. A representative cross-section of the sheet while folded and unfolded is shown in the inset to Fig. 2A. We find the mean curvature along the crease while loaded and unloaded, and plot them in Fig. 2A as a function of the stress σ corresponding to the applied force per unit length of crease and the sheet thickness. We observe that the curvatures for the folded and unfolded sheet evolve linearly as a function of applied stress over the typical range of curvatures observed in our crumpling experiments. Thus, even after loading is removed, a fraction proportional to the maximum loading applied can be identified, giving us confidence that the physical features of a crushed sheet can be still identified after the sheet is relaxed due to the residual plastic deformations.

Next, we perform measurements of the mean curvature of an unfolded sheet H^u for a typical crease as a function of number of folding and unfolding cycles for $\sigma = 0.7 \text{ Nmm}^{-2}$ applied for 30 seconds, before unfolding and placing the sheet on a flat-bed for scanning. As shown in Fig. 2B, we find that the curvature increases logarithmically with the number of applied loading cycles n , as $H^u = H_1^{un} + H_2^{un} \log(n)$ with a rate $H_2^{un} = 0.10 \text{ mm}^{-1}$. Because $\sigma = \chi^{-1} H^u$, and since $n \sim \omega t$, one can see there is analogy between the logarithmic observed here and those observed in time [24]. To probe this further, we measured the evolution of curvature when the applied load is applied over varying time interval t . As shown in Fig. 2C, we find that the increase in H^u with t is significantly lower compared with the increase in curvature with n over comparable cumulative loading time. Hence we find that the repeated folding and unfolding of the crease leads to far greater plastic deformations and is the dominant reason for the logarithmic increase in our

experiments. Thus, the evolution in our experiments appears to be consistent with memory observed due to cyclic driving in sheared suspensions [21, 38], and different from the time evolution reported previously in single folds and crumpled sheets [11, 12, 37].

IV. EVOLUTION OF CREASES

Figure 1B shows the regions with high H are organized along intersecting networks of creases with twist crumpling, visually similar to those which have been noted with other crumpling protocols [2, 13, 39]. To analyze the creases, we identify these regions where most of the plastic deformation in the sheet occurs (see SI Section IV). The total crease length ℓ normalized by L_0 as a function of n is plotted in Fig. 3A for various θ_f . We observe that it increases in all cases with number of cycles, and can be fitted by logarithm function $\ell = \ell_1 + \ell_2 \log(n)$, where ℓ_1 is the total crease length after the first loading cycle and ℓ_2 is the rate of growth corresponding to the creases with n . Both, ℓ_1 and ℓ_2 increase with ε , as shown in Fig. 3B,C, respectively.

In order to gain an understanding of the growth of the creases with loading, we studied complementary flat folding of a sheet into a smaller and smaller volume (see SI Section VI). These prescribed folding method allows us to not only estimate the total crease length but also practical differences due to folding a sheet with finite thickness. We define a compaction in this square folding case $\varepsilon_s = 1 - 1/m$, where L_0/m corresponds to length of the sides after m square folds and plot ℓ in Fig. 3A. In spite of the differences in definition of compaction, we find ℓ increases roughly over the same range of ℓ_1 as the sheet is folded to form smaller and smaller ordered squares as in twist crumpling. Growing disorder due to the thickness of the sheet results in a somewhat faster growth compared to the ideal square fold calculated limit.

A logarithmic growth of crease length has been reported in sheets crushed uniaxially inside a piston by Gottesman, *et al.* [13], but with a different two-parameter functional form. In those studies, the sheets were flattened after each cycle, and thus random perturbations were introduced which leads to the creation of new creases as the start point for the folding sequence is different. Indeed, if we introduce similar perturbations in our system, by unmounting and mounting after flipping the sheet inside out after each cycle, we find logarithmic growth as well, but with far greater rate of increase (see SI Section X) corresponding to the creation of larger numbers of fresh creases. Thus, our study finds that creases grow under repeated loading even when such random perturbations are absent due to the underlying plastic evolution of the sheet curvature under repeated loading. This evolution leads to sharpening curvature which then can exceed the thresholds used to identify creases and their observed growth.

We plot the distribution of crease length between branch points for various θ_f in Fig. 3D, and the mean ridge length in Fig. 3E. We find that the tails in the ridge length distribution $P(\ell_r)$ grows as the creases spread more broadly between the twisted ends with increasing θ_f as can be seen from Fig. 1B and Fig. S7. $P(\ell_r)$ for the various θ_f decay exponentially for sufficiently large ℓ_r , consistent with the gamma-distribution derived using a configurational entropy approach [40–42]. Further, the average crease length $\langle \ell_r \rangle$ increases initially with ε before reaching a broad peak and decreasing as the crushed volume continues to shrink. Plotting the number of ridges n_r versus cycle number n in Fig. 3F, we find that it grows consistent with a logarithmic function. Thus, we find that the total crease length grow because the total number of creases increase, even when $\langle \ell_r \rangle$ does not change significantly with n .

V. METASTABILITY

Since the full surface scans rely on dismounting the sheet after starting with a pristine sheet, it is only possible to understand statistical trends with those measurements. As a way to interrelate the crumpled configuration of the sheet after application of a training cycle, we examine the height profile $h(x, n)$ of the sheets along a length-wise section x after each cycle n . Representative evolution of a section of the sheet corresponding to $\theta = 180^\circ$, 360° , and 720° are shown in Fig. 4A-C, respectively. While the sections evolve rapidly in each case over the first tens of cycles, they converge to show a set of peaks and valleys which recur in the case of $\theta_f = 180^\circ$. Slow evolution of creases and appearance of new creases can be noted due to the evolving constraints [43] even as the sheet peaks and valleys mostly repeat and sharpen with n . It should be noted that new creases do not have to arise at that location, but changes in the structure elsewhere can also lead the sheet to move relative to the fixed section being examined. While, one notes similar trends in the case of $\theta_f = 720^\circ$, sudden rearrangements occur as well, whereby the entire cross-section undergoes a rapid snap-through event. Because the creases become sharper with increasing number of cycles, the number of creases in $h(x, n)$, identified by using a fixed curvature threshold criterion, continues to grow over $n = 1000$ even when reconfigurations are absent (see Fig. S10).

Thus, these observations further corroborate the discussion of the evolution of a single crease following Fig. 2B, i.e. plastic damage accumulates in regions which have sustained damage in previous cycles. As these constraints

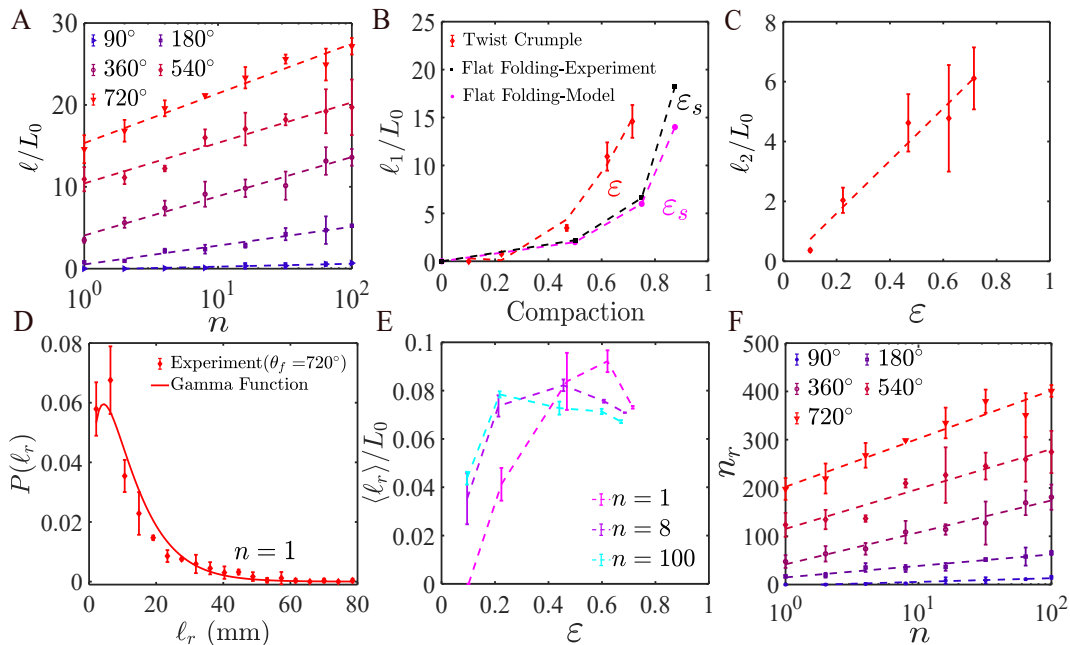


FIG. 3. Statistical evolution of creases with loading. (A) The evolution of the total crease length ℓ with n is well described by the logarithmic function $\ell = \ell_1 + \ell_2 \log(n)$. (B) The crease length after the first loading cycle ℓ_1 increases with compaction ε . The calculated and observed crease lengths when a sheet is folded into increasingly small squares plotted versus compaction ε_s estimated using the size of the folded sides. (C) The rate of increase of crease length ℓ_2 also increases with compression. (D) The distribution of crease length (ℓ_r) fitted with gamma function $P(\ell_r|\alpha, \beta) = \beta^\alpha \ell_r^{\alpha-1} \exp(-\beta \ell_r) / \Gamma(\alpha)$, where the fitted value of the shape parameter is $\alpha = 1.55$ and the scale parameter is $\beta = 7.84 \text{ mm}^{-1}$. (E) The average length of creases increases with compression as creases spread out from the central regions of the sheet, and then starts to decrease as the ridges are broken as the sheet is forced into a smaller volume. (F) The total number of ridges n_r increases logarithmically reflecting the growth in ℓ .

change, they can lead to both creation and destruction of creases as the curvature field adds pairs of peaks and valleys (see SI Fig. S11). Here we observe that the continuous evolution of the crease curvatures due to ageing can drive rapid reconfiguration of the crumpled structures even after the sheet structure repeats over hundreds of cycle even while evolving slowly. Thus, the picture which emerges from these observations is more subtle than the continuous approach to a limit cycle over tens of cycles shown by Shohat, *et al.* [23] with a precrumpled sheet subject to perturbative compression cycles. In particular bifurcation and deepening of the stability landscape can cause continuous evolution of the creases, as well as sudden transitions, respectively, as shown schematically in Fig. 4D.

To quantify the metastability, we computed a measure $\xi = \langle (h(x, n+2) - h(x, n))^2 \rangle_x$, where $\langle \dots \rangle_x$ corresponds to average over x and plot it in Fig. 4E in the case of $\theta_f = 720^\circ$. We observe that there are bursts of rearrangements after a large number of cycles where the sheet appears to converge to a stable structure. Further, these rearrangements show significant variations from trial to trial, with long periods of quiescence between large rearrangements. We quantify the relative intensity of the rearrangements over n by finding the number of peaks in ξ above a given threshold in the first, second and third part of the 1000 cycles, averaged over the three trials in the case of each θ_f . The number $\langle N_\xi \rangle$ is plotted in Fig. 4F and shows that the rearrangements for $\theta_f \leq 540^\circ$ eventually decrease and the folded shapes converge over time even as the creases sharpen. However, for large enough deformations corresponding to $\theta_f = 720^\circ$, the rearrangements can continue to occur even as they appear to converge over hundreds of cycles. In fact, we find that rearrangements persist in the case of $\theta_f = 720^\circ$ even as we performed trials with $n = 2000$ and the sheet started to tear along some of the creases due to the weakening caused by repeated plastic deformations (see SI Section IX). Thus, a recurrent folded structure does not always exist for large enough deformations as fatigue leads the sheet to progressively tear up.

The overall convergence to a limit cycle over a transient number of cycles that increase with increased θ_f is similar to that observed in cyclically sheared amorphous materials [22]. There, a relaxation to a limit cycle, and transitions between limit cycles was also observed with applied shear amplitude. For large enough amplitudes only irreversible migration of constituent particles was observed, suggesting a transition to chaos as in various dynamical systems [21, 22]. In particular the convergence of the folded structure and its evolution with increasing θ_f as captured in Fig. 4 can be noted to be similar. Our system, with the slow evolution of curvature folds with training cycle,

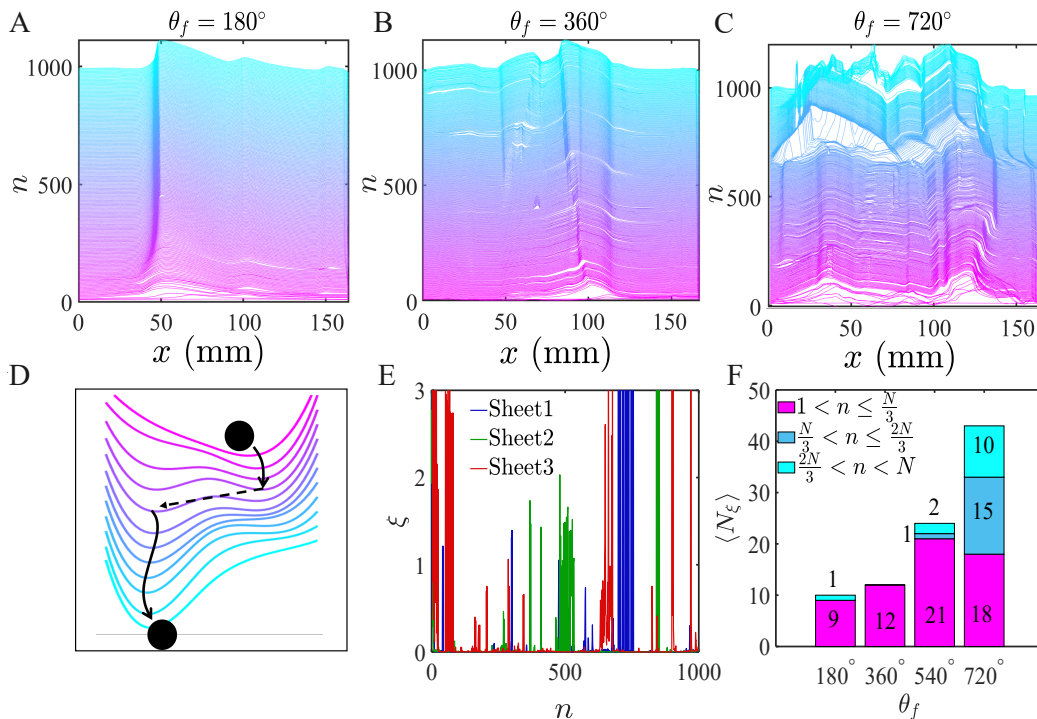


FIG. 4. Reversibility and irreversible transformation of sheet with training. (A-C) The evolution of a sheet cross section shows creases becoming sharper with n , and the formation of increasing number of new creases and sudden changes in the surface profile with increasing θ_f . (D) A schematic representation of the evolving energy landscape of the sheet which can give rise to slow evolution and rapid transitions in sheet structure. (E) ξ versus n shows spikes corresponding to changes in the profile ($\theta_f = 720^\circ$). (F) The number of peaks corresponding to reconfigurations increases with θ_f , but decreases with n for $\theta_f < 720^\circ$.

further indicates as well that the broad features of reversibility and irreversibility with applied amplitude can survive sufficiently slow evolution of fatigue in the system.

VI. CONCLUSIONS

In summary, we find that a repeatedly crumpled sheet can perform reversible transformations even as they are crushed significantly over a wide range of applied loading amplitudes. While temporal logarithmic relaxation has been noted in crumpled sheets, here we demonstrate logarithmic evolution of structure with training cycles which manifests itself in a wide range of measurable quantities. These include the evolution of the curvatures of the sheets, the crease length, the number length, and the crushed length reached with training cycles. Even when the system displaces metastability, we find that a convergent structure can be reached after a sufficiently large number of training cycles depending on the depth of the compression cycle. Our results echo the approach to limit cycle found in weakly perturbed pre-crumpled sheets [23], but significantly broaden our understanding of when reversible behavior can be expected. Our experiments demonstrate that elastoplastic sheets can satisfy the proposed deepening of the energy landscape which would give rise to programmable folding pathways leading to unique complex structures using origami [18]. However, for sufficiently large loading and compaction, a convergent structure is not reached even as tears develop as the sheet fatigues. Overall, we find that the behavior of crumpled sheet under repeated loading is similar to other disordered system, and in particular the reversible transformation of athermal particles subjected to cyclic shear [21, 22, 38]. There, reversibility is observed for a range of sufficiently small strain amplitude, but irreversibility develops with increasing amplitude depending on the Lyapunov exponents of the system. While, a similar analysis is beyond the scope of this study, it may be anticipated that our results can stimulate work in that direction.

METHODS

A. Materials and Apparatus

Biaxially oriented polyethylene terephthalate (BoPET), also known as Mylar, sheets of length $L_0 = 16.5$ cm, width $W_0 = 16.5$ cm, and thickness $h_0 = 90 \mu\text{m}$ were used in the study. These sheets have a bending modulus $E = 4.16$ GPa, obtained with standard beam bending measurements. The sheet is rolled and clamped onto two circular rigid aluminum disks of diameter $D = 52.5$ mm to form a cylinder of length L_0 . The axis of one end is twisted axially with a Parker stepper motor systems controlled by a computer through an angle θ with a rate $\omega = 3.67$ degrees/s. Thus, a loading cycle takes approximately 6 minutes and 30 seconds when θ is increased to $\theta_f = 720^\circ$ and then returned back to 0° . The other end is not allowed to twist, but allowed to move along its axis while mounted on low-friction linear guides ($\lesssim 0.3N$). Although an axial load can be prescribed, we perform measurements while allowing the sheet to contract or expand freely.

B. Laser Profilometry

The surface profile of the sheet is obtained by illuminating the sheet with a 640 nm red laser sheet orthogonal to the unperturbed surface. The illuminated surface is then imaged at an angle with a Pixelink digital camera with a resolution of 2592×2048 pixels. The bright pixels are used to locate the surface with a centroid algorithm to within a few microns. This method yields a single height profile along the length of the sheet while mounted on the apparatus. To obtain a full scan of the sheet surface, the sheet is unmounted to relieve elastic stresses. It is then placed on a flat scanner bed after being flattened somewhat to remove overhangs. Care is taken to minimize introducing plastic deformations in the process. Because the sheet cannot be remounted to have the same boundary conditions as when it was dismounted, we start with a fresh sheet for each scan while measuring as a function of n or θ_f .

Acknowledgements

This work was supported under U.S. National Science Foundation grant DMR-2005090.

-
- [1] M. Ben Amar and Y. Pomeau. Crumpled paper. *Proceedings: Mathematical, Physical and Engineering Sciences*, 453(1959):729–755, 1997.
 - [2] Daniel L. Blair and Arshad Kudrolli. Geometry of crumpled paper. *Phys. Rev. Lett.*, 94:166107, Apr 2005.
 - [3] L. Boué, M. Adda-Bedia, A. Boudaoud, D. Cassani, Y. Couder, A. Eddi, and M. Trejo. Spiral patterns in the packing of flexible structures. *Phys. Rev. Lett.*, 97:166104, Oct 2006.
 - [4] T. A. Witten. Stress focusing in elastic sheets. *Rev. Mod. Phys.*, 79:643–675, Apr 2007.
 - [5] Andrew Croll, Timothy Twohig, and Theresa Elder. The compressive strength of crumpled matter. *Nature Communications*, 10:1502, 04 2019.
 - [6] Kittiwit Matan, Rachel B. Williams, Thomas A. Witten, and Sidney R. Nagel. Crumpling a thin sheet. *Phys. Rev. Lett.*, 88:076101, Jan 2002.
 - [7] M. C. Fokker, S. Janbaz, and A. A. Zadpoor. Crumpling of thin sheets as a basis for creating mechanical metamaterials. *RSC Adv.*, 9:5174–5188, 2019.
 - [8] Shankar C. Venkataramani. Buckling sheets open a door to understanding self-organization in soft matter. *Proceedings of the National Academy of Sciences*, 116(5):1477–1479, 2019.
 - [9] B.N.J. Persson. *Sliding Friction: Physical Principles and Applications*. NanoScience and Technology. Springer Berlin Heidelberg, 2013.
 - [10] E. Bertin, Jean-Philippe Bouchaud, J-M Drouffe, and C Godreche. The kovacs effect in model glasses. *Journal of Physics A General Physics*, 36, 06 2003.
 - [11] B. Thiria and M. Adda-Bedia. Relaxation mechanisms in the unfolding of thin sheets. *Phys. Rev. Lett.*, 107:025506, Jul 2011.
 - [12] Ariel Amir, Yuval Oreg, and Yoseph Imry. On relaxations and aging of various glasses. *Proceedings of the National Academy of Sciences*, 109(6):1850–1855, 2012.
 - [13] Omer Gottesman, Jovana Andrejevic, Chris H. Rycroft, and Shmuel M. Rubinstein. A state variable for crumpled thin sheets. *Communications Physics*, 1(1):70, 2018.
 - [14] Nathan C. Keim, Joseph D. Paulsen, Zorana Zeravcic, Srikanth Sastry, and Sidney R. Nagel. Memory formation in matter. *Rev. Mod. Phys.*, 91:035002, Jul 2019.
 - [15] B. A. DiDonna and T. A. Witten. Anomalous strength of membranes with elastic ridges. *Phys. Rev. Lett.*, 87:206105, Oct 2001.

- [16] Christian D. Santangelo. Extreme mechanics: Self-folding origami. *Annual Review of Condensed Matter Physics*, 8(1):165–183, 2017.
- [17] Menachem Stern, Chukwunonso Arinze, Leron Perez, Stephanie E. Palmer, and Arvind Murugan. Supervised learning through physical changes in a mechanical system. *Proceedings of the National Academy of Sciences*, 117(26):14843–14850, 2020.
- [18] Menachem Stern, Viraa Jayaram, and Arvind Murugan. Shaping the topology of folding pathways in mechanical systems. *Nature Communications*, 9:4303, 2018.
- [19] Chukwunonso Arinze, Menachem Stern, Sidney R. Nagel, and Arvind Murugan. Learning to self-fold at a bifurcation. *Phys. Rev. E*, 107:025001, Feb 2023.
- [20] Edmund R. Nowak, James B. Knight, Eli Ben-Naim, Heinrich M. Jaeger, and Sidney R. Nagel. Density fluctuations in vibrated granular materials. *Phys. Rev. E*, 57:1971–1982, Feb 1998.
- [21] David Pine, J Gollub, J Brady, and Alexander Leshansky. Chaos and threshold for irreversibility in sheared suspensions. *Nature*, 438:997–1000, 2005.
- [22] Ido Regev, Turab Lookman, and Charles Reichhardt. Onset of irreversibility and chaos in amorphous solids under periodic shear. *Phys. Rev. E*, 88:062401, Dec 2013.
- [23] Dor Shohat, Daniel Hexner, and Yoav Lahini. Memory from coupled instabilities in unfolded crumpled sheets. *Proceedings of the National Academy of Sciences*, 119(28), 2022.
- [24] Théo Jules, Austin Reid, Karen E. Daniels, Muhittin Mungan, and Frédéric Lechenault. Delicate memory structure of origami switches. *Phys. Rev. Res.*, 4:013128, Feb 2022.
- [25] Yutong Xia, Narayanan Kidambi, Evgueni Filipov, and K. W. Wang. Deployment Dynamics of Miura Origami Sheets. *Journal of Computational and Nonlinear Dynamics*, 17(7):071005, 04 2022.
- [26] Francis Dunne, Kjell Westra, Caleb Mattox, and Jacob Leachman. Fatigue life characterization of hand folded and vacuum formed kresling origami bellows at 77k. *IOP Conference Series: Materials Science and Engineering*, 1241(1):012014, may 2022.
- [27] T. Tallinen, J. A. Åström, and J. Timonen. The effect of plasticity in crumpling of thin sheets. *Nature materials*, 8 1:25–9, 2009.
- [28] Mehdi Habibi, Mokhtar Adda-Bedia, and Daniel Bonn. Effect of the material properties on the crumpling of a thin sheet. *Soft Matter*, 13:4029–4034, 2017.
- [29] Handika Dany Rahmayanti, Fisca Dian Utami, and Mikrajuddin Abdullah. Physics model for wringing of wet cloth. *European Journal of Physics*, 37(6):065806, sep 2016.
- [30] Pan Dong, Mengfei He, Nathan C. Keim, and Joseph D. Paulsen. Twisting a cylindrical sheet makes it a tunable locking material. *Phys. Rev. Lett.*, 131:148201, Oct 2023.
- [31] Giles W. Hunt and Ichiro Ario. Twist buckling and the foldable cylinder: an exercise in origami. *International Journal of Non-Linear Mechanics*, 40(6):833–843, 2005.
- [32] Li-Min Wang, Sun-Ting Tsai, Chih-yu Lee, Pai-Yi Hsiao, Jia-Wei Deng, Hung-Chieh Fan Chiang, Yicheng Fei, and Tzay-Ming Hong. Crumpling-origami transition for twisting cylindrical shells. *Phys. Rev. E*, 101:053001, May 2020.
- [33] L. H. Donnell. Stability of thin-walled tubes under torsion. Technical report, National Advisory Committee for Aeronautics - Report No. 479, 1933.
- [34] Gerard Giménez-Ribes, Melika Motaghian, Erik van der Linden, and Mehdi Habibi. Crumpled structures as robust disordered mechanical metamaterials. *Materials & Design*, 232:112159, 2023.
- [35] Julien Chopin and Arshad Kudrolli. Tensional twist-folding of sheets into multilayered scrolled yarns. *Science Advances*, 8(14):eabi8818, 2022.
- [36] T. Jules, F. Lechenault, and M. Adda-Bedia. Plasticity and aging of folded elastic sheets. *Phys. Rev. E*, 102:033005, Sep 2020.
- [37] Dor Shohat, Yaniv Friedman, and Yoav Lahini. Logarithmic aging via instability cascades in disordered systems. *Nature Physics*, 19(12):1890–1895, 2023.
- [38] Joseph D. Paulsen, Nathan C. Keim, and Sidney R. Nagel. Multiple transient memories in experiments on sheared non-brownian suspensions. *Phys. Rev. Lett.*, 113:068301, Aug 2014.
- [39] Anne Dominique Cambou and Narayanan Menon. Three-dimensional structure of a sheet crumpled into a ball. *Proceedings of the National Academy of Sciences*, 108(36):14741–14745, 2011.
- [40] Eric Sultan and Arezki Boudaoud. Statistics of crumpled paper. *Phys. Rev. Lett.*, 96:136103, Apr 2006.
- [41] Alexander S. Balankin and Leonardo Flores-Cano. Edwards’s statistical mechanics of crumpling networks in crushed self-avoiding sheets with finite bending rigidity. *Phys. Rev. E*, 91:032109, Mar 2015.
- [42] Jovana Andrejevic, Lisa M. Lee, Shmuel M. Rubinstein, and Chris H. Rycroft. A model for the fragmentation kinetics of crumpled thin sheets. *Nature Communications*, 12(1), Mar 2021.
- [43] Arezki Boudaoud, Pedro Patrício, Yves Couder, and Martine Ben Amar. Dynamics of singularities in a constrained elastic plate. *Nature*, 407:718–20, 11 2000.
- [44] S. Kodama and N. Yamaki. Postbuckling behavior of pressurized circular cylindrical shells under torsion—ii. theory. *International Journal of Non-Linear Mechanics*, 16(3):355–370, 1981.
- [45] Wesley Wong and Sergio Pellegrino. Wrinkled membranes, part ii: Analytical models. *Journal of Mechanics of Materials and Structures*, 1:27–61, 2006.
- [46] John W. Harris and Horst Stöcker. *Handbook of Mathematics and Computational Science*. Springer, New York, 1998.
- [47] Hongxun Song, Weixing Wang, Fengping Wang, Linchun Wu, and Zhiwei Wang. Pavement crack detection by ridge detection on fractional calculus and dual-thresholds. *International Journal of Multimedia and Ubiquitous Engineering*,

10:19–30, 2015.

- [48] S. Deboeuf, E. Katzav, A. Boudaoud, D. Bonn, and M. Adda-Bedia. Comparative study of crumpling and folding of thin sheets. *Phys. Rev. Lett.*, 110:104301, Mar 2013.

Supplementary Information

I. WRINKLING INSTABILITY AND DEVELOPMENT OF FOLDS

According to Donnell's stability analysis of thin-walled elastic tubes under torsion [33, 44], the number of wrinkles,

$$N_w = N_0 \left[\frac{1}{\sqrt{1-\mu^2}} \frac{L_0^2 h}{D^3} \right]^{-1/4}, \quad (\text{S1})$$

where $N_0 = 2.62$, and μ is the Poisson ratio, which is approximately 0.5 in the case of Mylar. Fitting the data, we find $N_0 = 1.76$, corresponding to a systematically lower number of wrinkles. The difference is likely due to the fact that a cylindrical rolled sheet, rather than a cylindrical shell, is twisted in the experiments. Based on work reported in the case of sheared planar sheets [45], stress relaxation near the free edges can lead to the angles that the wrinkles make with the direction of shear to change, lowering the number of wrinkles. This fact also leads to disorder in the formation of the slanted folds in the case of higher aspect ratio cylinders, as opposed to those in thin cylindrical shells, where they are ordered for a wide range of aspect ratios even as applied twist is increased [33].

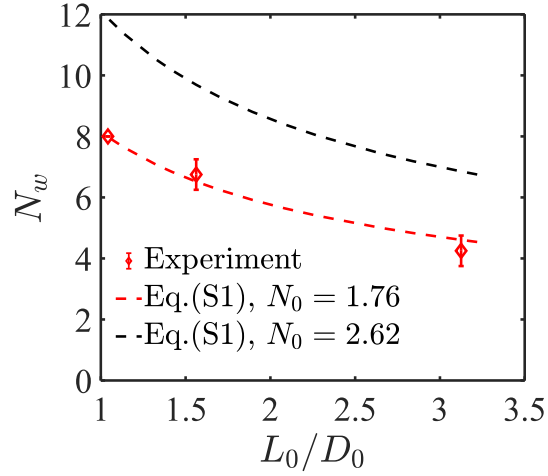


FIG. S1. The number of wrinkles N_w observed as a function of L_0/D_0 and compared with Eq. (S1).

II. HYPERBOLIC HYPERBOLOID

If the sheet was replaced by a set of infinitely thin inextensible filaments of length L_0 arranged cylindrically with diameter D_0 , they would give rise to a hyperbolic hyperboloid when twisted up to $\theta < 180^\circ$ [46]. Then, the distance between the ends as a function of twist θ is given by

$$L/L_0 = \sqrt{1 - \left(\frac{D_0}{L_0}\right)^2 \sin^2(\theta/2)}. \quad (\text{S2})$$

Plotting L/L_0 over the range $0 \leq \theta \leq \pi/2$ in Fig. S2, we find that it is systematically higher than the end to end distance measured in the case of the sheet.

As shown in Fig. 1, the deformation is initially localized in the central portion of the structure. We can model the deformation before self-contact as being localized to a central portion of the cylinder ϕL_0 , with essentially straight sections near the clamped edges. Then, we have

$$L/L_0 = (1 - \phi) + \phi \sqrt{1 - \left(\frac{D_0}{\phi L_0}\right)^2 \sin^2(\theta/2)}, \quad (\text{S3})$$

where $\phi = 1$ corresponds to Eq. (S2). By fitting, we find $\phi \approx 0.29$, which corresponds to the twist being effectively localized to the central 30% of the cylinder which roughly consistent with the image of the deformation shown in Fig. 1A corresponding to $\theta = 90^\circ$.

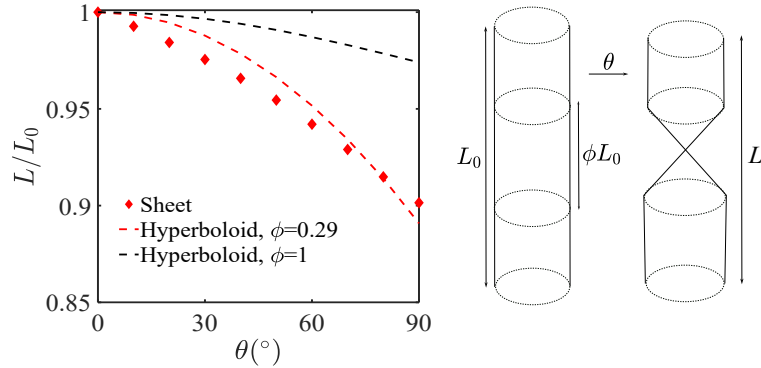


FIG. S2. The measured end to end distance between clamped edges L as a function of twist angle θ . Comparison with Eq. (S3) with $\phi = 1$ and $\phi = 0.29$ are also shown.

III. HYSTERESIS CHARACTERISTICS

Figure S3 shows a plot of the compressed length L_c when the sheet is twisted by θ , and then the length L_n after untwisting. L_c decreases rapidly after the first cycle, and then increases slowly with n (see Fig. S3C). L_n decreases relatively more rapidly with increasing n as θ_f is increased (see Fig. S3E).

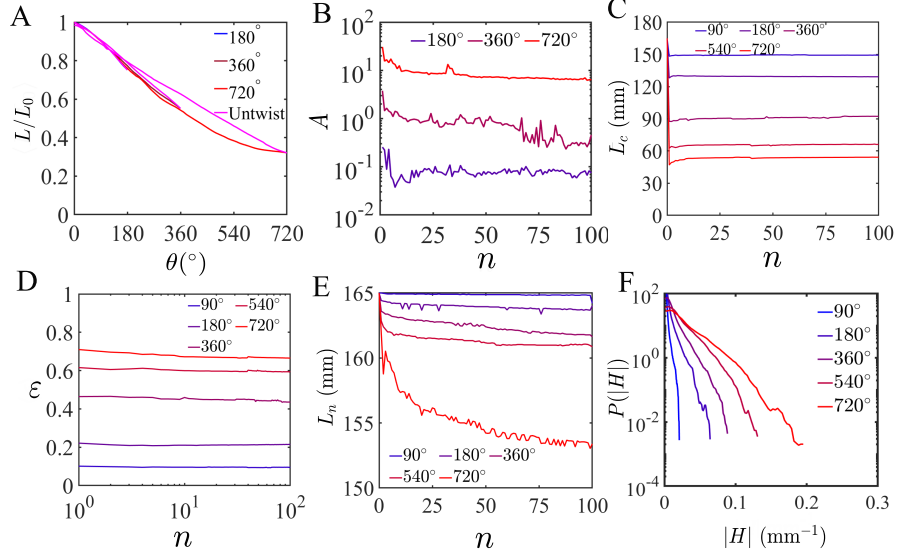


FIG. S3. (A) L/L_0 as a function of θ in the case of three different θ_f corresponding to $n = 1$. While the path followed during twist is the same, the return path during the untwisting varies leading to growing differences with θ_f . (B) The area enclosed by the hysteresis curve as a function of n for each case of θ_f . The hysteresis decreases slowly with n . The noise floor is approximately 10^{-1} for these measurements, similar to A measured in the case of $\theta_f = 180^\circ$. The compressed length L_c versus n (C), and the corresponding strain ϵ versus n (D). (E) The end to end length after each cycle L_n observed as a function of loading cycle n . (F) The mean curvature distribution $P(|H|)$ becomes broader with increasing θ_f as the sheet is increasingly deformed.

IV. CREASE DETECTION

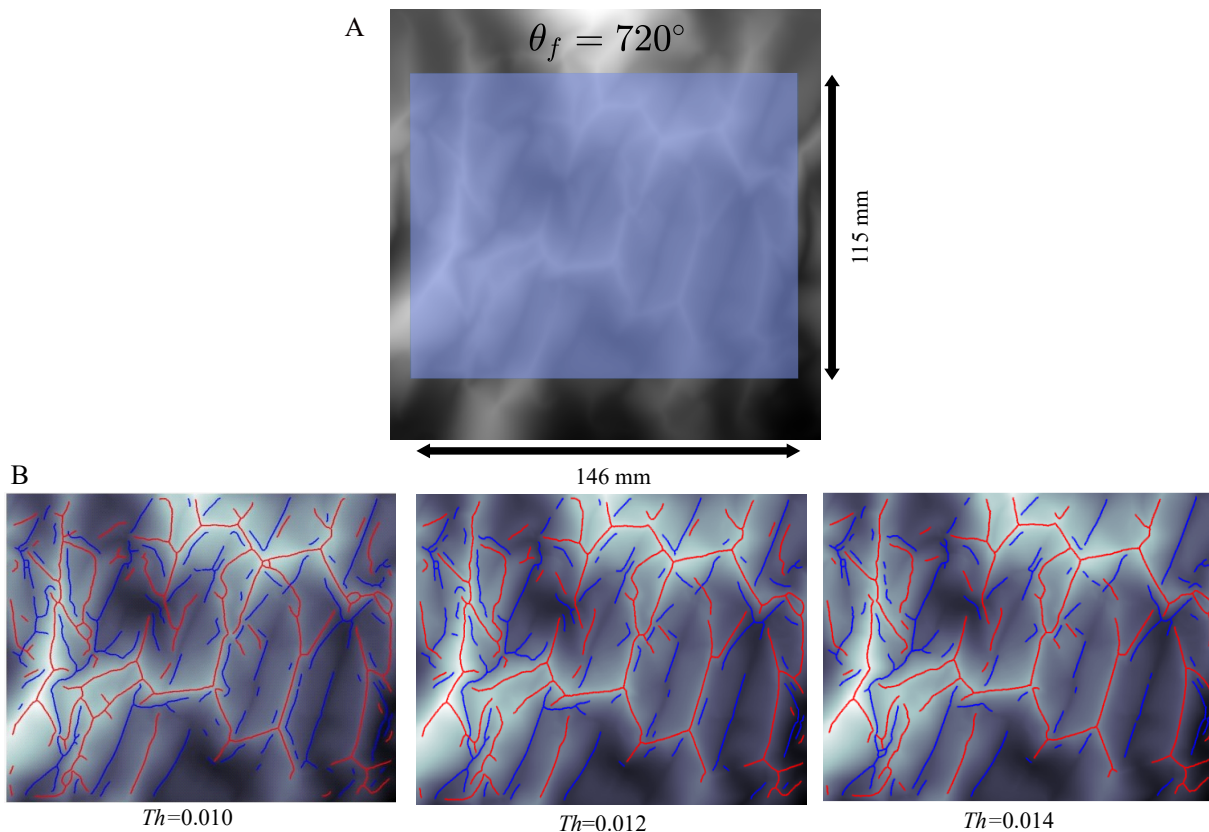


FIG. S4. (A) The region of interest (ROI) considered for the statistical analysis. (B) The creases longer than 2 mm, detected assuming global thresholds $Th = 0.010$, $Th = 0.012$, and $Th = 0.014$. The blue (red) lines correspond to valleys (ridges).

A. Pixel Dimensions and Image Resizing

We first examine the total number of rows and columns in the matrix Z with the scan data. If the number of rows exceeds the number of columns, we increase the number of columns, transforming the pixel dimensions into a square shape aligned with the initial pixel dimension along the rows. The same process is applied in reverse if the number of columns is greater than the number of rows. For example, if one has a matrix Z with order $R \times C$ and $R > C$, and the pixel dimension is $r \times c$ along the row and columns respectively, then we make the pixel dimension square by changing the number of columns to:

$$N_{\text{new}} = \frac{c \times C}{r} \quad (\text{S4})$$

and vice versa. In this case, the individual pixel dimension becomes $r \times r$. We resize the image as needed. In our case, the image is resized by a factor of 0.5.

B. Valley Detection

This is the main part of the ridge detection process. We define a two-dimensional array having a size equal to the size of the Z matrix with all elements initialized to zero. Our goal is to set elements to 1 at positions where there are creases. Creases are extracted by applying two levels of thresholds: firstly, in the local level, and then in the global level [47].

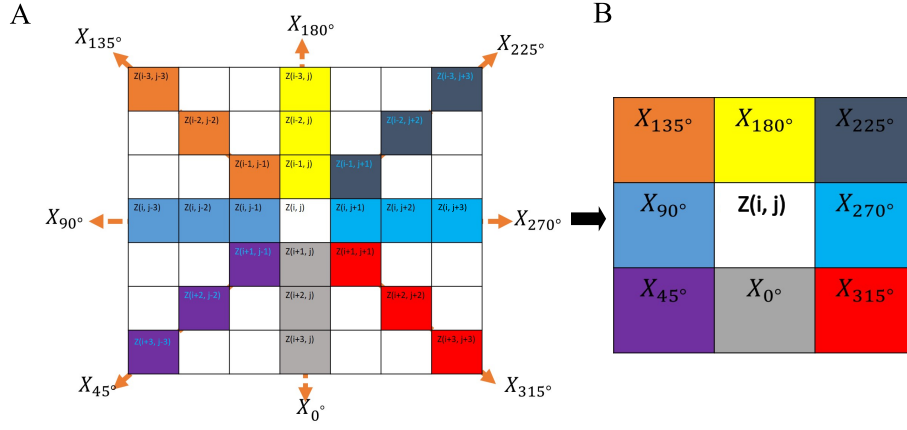


FIG. S5. (A) The 7×7 matrix illustrating the selection of the neighbors along eight different directions to obtain weighted means ($X_0^\circ, X_{45^\circ}, X_{90^\circ}, X_{135^\circ}, X_{180^\circ}, X_{225^\circ}, X_{270^\circ}, X_{315^\circ}$). (B) The resulting matrix A containing the 8 weighted means from the nearest 8 neighbors of the target pixel is calculated using the weighted mean formula for three consecutive pixels along a given direction.

- The weighted mean along eight directions ($0^\circ, 45^\circ, 90^\circ, 135^\circ, 180^\circ, 225^\circ, 270^\circ, 315^\circ$), as shown in Figure S5, are calculated from the three consecutive matrix elements along that direction:

$$X_0 = \frac{Z(i+1, j) + v \times Z(i+2, j) + \frac{v(v+1)}{2} \times Z(i+3, j)}{W_{\text{factor}}}, \quad (\text{S5})$$

$$X_{45} = \frac{Z(i+1, j-1) + v \times Z(i+2, j-2) + \frac{v(v+1)}{2} \times Z(i+3, j-3)}{W_{\text{factor}}}, \quad (\text{S6})$$

$$X_{90} = \frac{Z(i, j-1) + v \times Z(i, j-2) + \frac{v(v+1)}{2} \times Z(i, j-3)}{W_{\text{factor}}}, \quad (\text{S7})$$

$$X_{135} = \frac{Z(i-1, j-1) + v \times Z(i-2, j-2) + \frac{v(v+1)}{2} \times Z(i-3, j-3)}{W_{\text{factor}}}, \quad (\text{S8})$$

... and so on.

Where the weighted factor $W_{\text{factor}} = 1 + v + \frac{v(v+1)}{2}$ is used with a suitable value of v . In our case, we have set it to be 20.

- From the 7×7 matrix, we create a 3×3 matrix (denoted as A) with the central pixel value as the original height and other neighboring elements with a weighted mean along corresponding directions, as shown in Fig. S5.
- Define the local threshold value (Th_{local}) by the following formula:

$$Th_{\text{local}} = \frac{\text{mean}(A) - Z(i, j)}{2}. \quad (\text{S9})$$

- From the 3×3 matrix A , we construct a new 1×4 matrix, denoted as G . To achieve this, we introduce a local threshold value as a reference. In the process, we define pairs of mean values in opposite corners as $X_{s \times 45^\circ}$ and $X_{s \times 45^\circ + 180^\circ}$ for $s = 0$ to $s = 4$. The matrix G is defined as $G = [g_s]_{(s=1,2,3,4)} = [g_1, g_2, g_3, g_4]$, where g_s is calculated as:

$$g_s = \frac{(X_{s \times 45^\circ + 180^\circ} - Z(i, j)) + (X_{s \times 45^\circ} - Z(i, j))}{2}, \quad (\text{S10})$$

if $|(X_{s \times 45^\circ + 180^\circ} - Z(i, j))| > Th_{\text{local}}$ or $|(X_{s \times 45^\circ} - Z(i, j))| > Th_{\text{local}}$. Otherwise, $g_s = 0$.

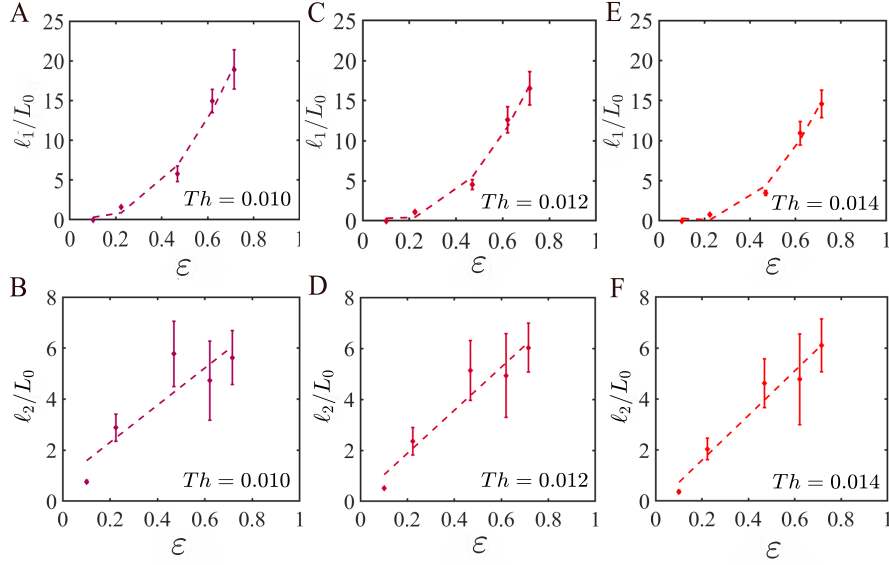


FIG. S6. The effect of the global threshold Th on measured evolution parameters of the crease network.

- Now we implement the global thresholding step to decide if the central pixel is a valley or not by comparing the maximum value of matrix G with the global threshold value Th . If $\max(G) > Th$, then $\text{Valley}(i, j) = 1$. Otherwise, $\text{Valley}(i, j) = 0$. In our case, we have used Th : 0.010, 0.012, and 0.014, and tested to check their effect of crease detection and effect on statistical values of interest.

We invert the surface and apply the same algorithm to then extract the ridge network. An example of the ridge and valley detected using various thresholds is shown in Fig. S4.

C. Crease Length Calculation

We count the number of occupied pixels N_{occupied} and apply the following formula to estimate the crease length:

$$\ell = N_{\text{occupied}} \times \frac{\sqrt{2} + 1}{2} \times r \quad (\text{S11})$$

Where ℓ is the ridge length, r is the pixel dimension. While writing Equation S11, we have considered that 50% of the non-zero pixels are connected diagonally, and the remaining 50% linearly.

As shown in Fig. S6, while the choice of threshold varies the values somewhat, the trends as quantified by ℓ_1 and ℓ_2 remain robust.

V. SPATIAL DISTRIBUTION OF CURVATURE

We plot the average $|H|$ as a function of distance from one clamped end to the other in Fig. S7. As can be seen from Fig. S7A,B, H is lower near in the clamped edges because the sheet is forced to maintain the curvature of the end disks on which it is mounted. When the sheet is repeatedly twisted, H increase systematically everywhere and thus the variation across x persists (see Fig. S7C,D). Accordingly, we analyze the distribution of the measured H over a 145 mm by 115 mm centrally cropped area of the sheet to avoid direct boundary effects.

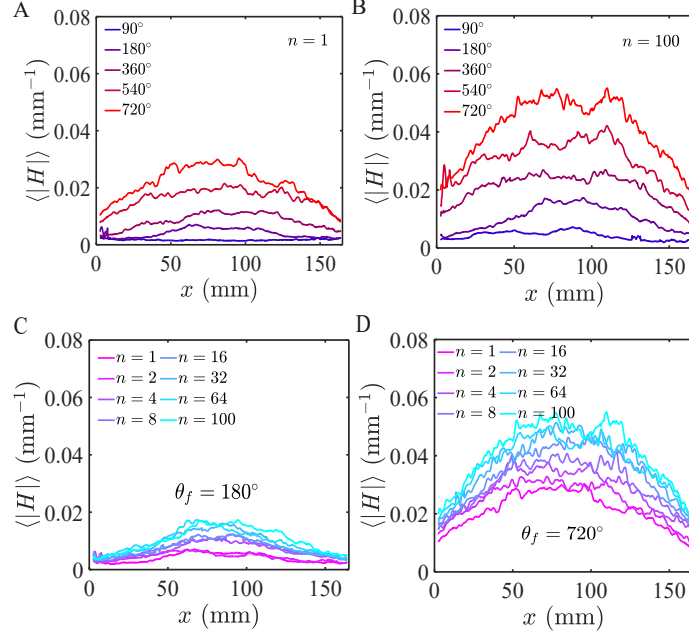


FIG. S7. Mean curvature of the crumpled sheet as a function of distance along the sheet's length for various θ_f after cycle $n = 1$ (A) and $n = 100$ (B), respectively. (C,D) Mean curvature of the cross section as a function of distance along the sheet's length for increasing n for $\theta_f = 180^\circ$ and 720° , respectively. The sheet is more crumpled in the central regions between the clamps where sheet forms a tight bundle when twisted.

VI. FOLDING MODEL OF CREASES

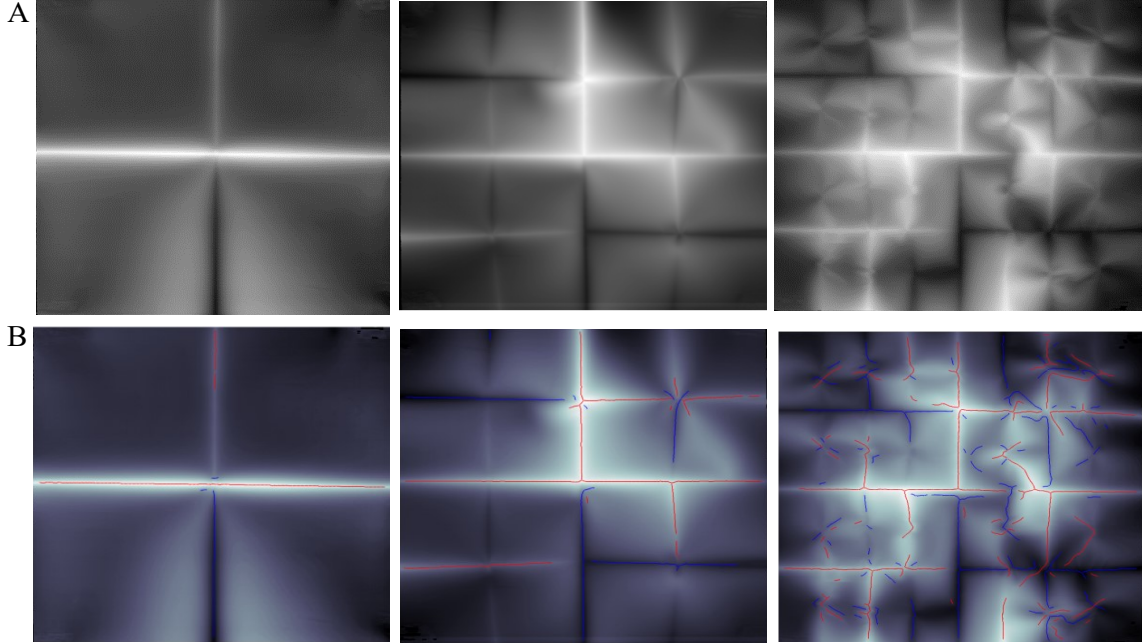


FIG. S8. (A) Folds become increasingly disordered as the sheet is folded into smaller squares. (B) The detected ridges and valleys are superimposed on the scans. Note that refolded creases become sharper and are detected more fully as their curvature exceeds the threshold used to detect a crease.

We performed complementary studies of crease growth using flat folding methods [48]. First, we consider a square infinitesimally thin sheet with side L_0 , and calculate the total crease length upon flat folding the sheet into smaller squares with sides L_0/m , with $m = 1, 2, 4, \dots$. This flat folded sheet can fit inside a piston corresponding compression $\varepsilon_s = 1 - 1/m$, and used to plot calculated ℓ in Fig. 3B.

Then, to understand the impact of sheet thickness and the crease detection methods, we also performed the same square folding with $L_0 \times L_0$ Mylar sheets for $m = 1, 2$, and 4. The scans are shown in Fig. S8, and show the growing disorder and nonuniformity of the curvature along the creases even though they were folded by an ordered sequence of folds. Plotting the average mean curvature of the sheet $\langle |H| \rangle$ in Fig. S9, we observe that it increases to a similar degree as the sheet is progressively folded and thus compressed to contain within a piston which has been strained through ε .

Next, we use the same threshold criteria used to detect the ridges as in the twist experiments. Examining the detected ridge and valleys superposed on the scans shown in Fig. S8(B), we observe that primary folds which was missed initially was detected in their entirety with subsequent refolding. However, the new folds corresponding to $m = 2, 3$ have overall lower curvature and were detected to a lower degree.

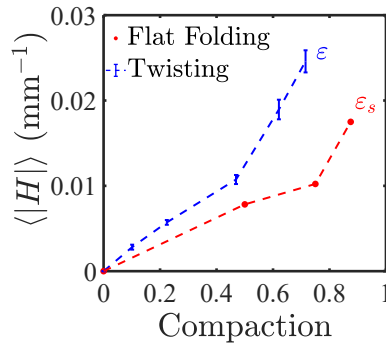


FIG. S9. The absolute mean curvature of the sheet increases with the compaction in both flat folding and twist crumpling cases.

Because of the thickness of the sheet, the sheet becomes increasingly more difficult to fold, with increasing number of folds. Further, one observes the appearance of curvature with opposite signs adjacent to the square folds as the sheet is forced back to a planar configuration. While overall smaller in magnitude, they can be noted to be similar in magnitude to the creases created further along the folding sequence. One can further observe the appearance of disorder and creases at the intersection of the creases created while folding, earlier in the sequence.

Thus, while not all the creases expected corresponding to an ideal square folding are detected as they elastically relax below the criteria set for detecting ridges once unfolded to perform the scans, additional creases are created due to the unfolding process of a sheet with finite thickness as illustrated in Fig. S8. As seen from the comparison for the total ridge length ℓ shown in Fig. 3B, these counter trends are observed to lead to an overall higher total crease length in the experimentally obtained case compared to the ideal square folds.

VII. EVOLUTION OF CREASES WITH TRAINING CYCLES

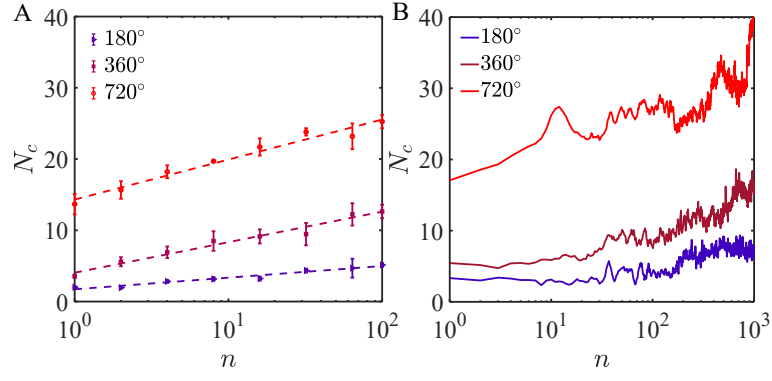


FIG. S10. The total number of creases counted along the length of the cylinder evolves logarithmically with the loading cycles obtained from the scanned surfaces (A), and using the cross-sections measured after each cycle (B).

VIII. BIFURCATION AND MERGING OF FOLDS

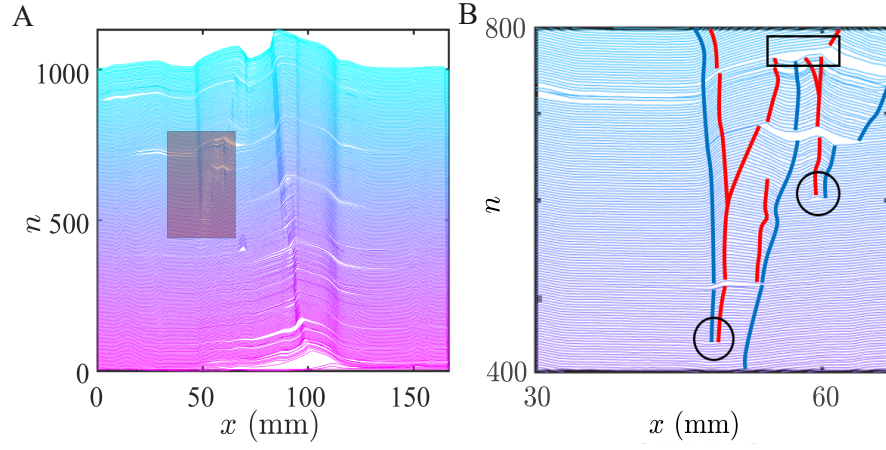


FIG. S11. (A) The evolution of a cross-section with n for $\theta_f = 360^\circ$. (B) A zoomed in view of the shaded region in Fig. S11(A) showing the relative motion of the creases with increasing n , including creation of peak and valley pairs (black circles) and destruction of creases (black rectangle).

IX. FATIGUE WITH CYCLE NUMBER

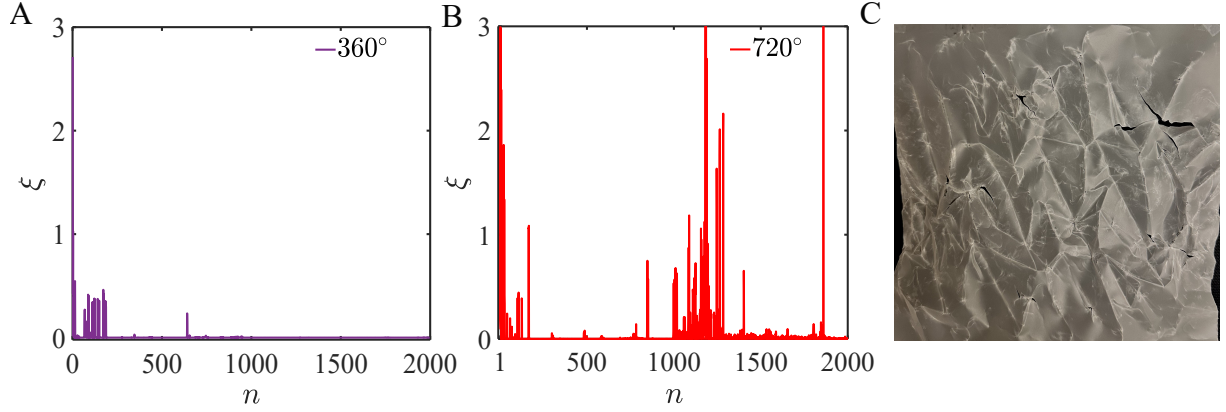


FIG. S12. ξ tracking over the first 2000 cycles for two different cases, $\theta_f = 360^\circ$ (A) and 720° (B). (C) An image of the sheet after $n = 2000$ twisting cycles shows tears along some of the creases ($\theta_f = 720^\circ$).

Fig. S12 shows how the different loading condition affect the configuration of the system even after thousands of repeated cycles. In the case of $\theta_f = 360^\circ$, we observe that ξ decreases to zero and stays that way after few hundred cycles even as n is increased to 2000. Whereas, in the case of $\theta_f = 720^\circ$, we observe that ξ continues to large spikes indicating large rearrangements over the entire range of n . The sheets is observed to show cracks or tears along some of the repeatedly folded creases at approximately $n = 1800$. Thus, no convergence of structure is observed even as fatigue sets in over the course of the applied cycles.

X. EFFECT OF INTER-CYCLE PERTURBATIONS

In order to test the effect of introducing random perturbations between training cycles, we performed experiments where we unmounted the sheet after each cycle and then remounted it after flipping the cylindrical sheet surface inside out. This can lead to a different folding sequence as the sheet compresses since the applied constraints progress differently in detail. As shown in Fig. S13, we find that the damage grows logarithmically as well, but with a significantly higher growth rate $\ell_2/L_0 = 11.2$, as opposed to 4.8, when the sheet is simply twisted repeatedly without imposing any inter-cycle perturbations.

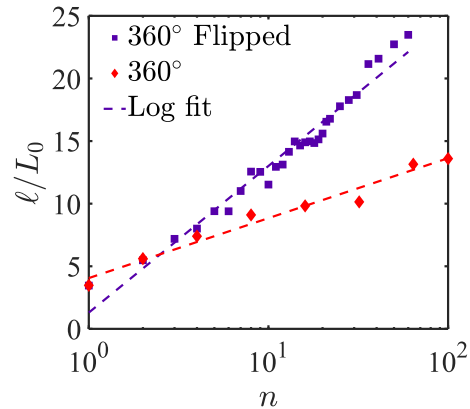


FIG. S13. ℓ/L_0 for $\theta_f = 360^\circ$ with two distinct crumpling protocols: one involving the flipping the sheet surface after each iteration and the other keeping the sheet clamped without unmounting throughout the experiments. The graph exhibits a higher rate of increase, with $\ell_2/L_0 = 11.2$, in the former case, whereas the rate is 4.8 in the latter case.

XI. SUPPLEMENTARY MOVIES

1. [Supplementary Movie S1](#): A movie of a sheet as it is twisted twice about its axis through $\theta_f = 720^\circ$. Crumples develop as the sheet buckles and folds with applied twist and gives rise to plastic deformations.
2. [Supplementary Movie S2](#): Snapshots of the sheet after the application of a loading cycle over 100 cycles corresponding to $\theta_f = 720^\circ$. The creases are observed to largely repeat but a few new creases and sheet reconfigurations can be also observed.